Clinical Chemistry 65:10
1276–1286 (2019)

Prognostic Relevance of Steroid Sulfation in Adrenocortical Carcinoma Revealed by Molecular Phenotyping Using High-Resolution Mass Spectrometry Imaging

Na Sun,[1*†] Thomas Kunzke,[1*†] Silviu Sbiera,[2] Stefan Kircher,[3] Annette Feuchtinger,[1] Michaela Aichler,[1] Sabine Herterich,[4] Cristina L. Ronchi,[2,5] Isabel Weigand,[2] Nicolas Schlegel,[6,7] Jens Waldmann,[8] Maria Candida Villares Fragoso,[9] Timothy G. Whitsett,[10] Anthony J. Gill,[11] Martin Fassnacht,[2,4,7] Axel Walch,[1] and Matthias Kroiss[2,4,7*]

BACKGROUND: Adrenocortical carcinoma (ACC) is a rare tumor with variable prognosis even within the same tumor stage. Cancer-related sex hormones and their sulfated metabolites in body fluids can be used as tumor markers. The role of steroid sulfation in ACC has not yet been studied. MALDI mass spectrometry imaging (MALDI-MSI) is a novel tool for tissue-based chemical phenotyping.

METHODS: We performed phenotyping of formalin-fixed, paraffin-embedded tissue samples from 72 ACC by MALDI-MSI at a metabolomics level.

RESULTS: Tumoral steroid hormone metabolites—estradiol sulfate [hazard ratio (HR) 0.26; 95% CI, 0.10–0.69; $P = 0.005$] and estrone 3-sulfate (HR 0.22; 95% CI, 0.07–0.63; $P = 0.003$)—were significantly associated with prognosis in Kaplan–Meier analyses and after multivariable adjustment for age, tumor stage, and sex (HR 0.29; 95% CI, 0.11–0.79; $P = 0.015$ and HR 0.30; 95% CI, 0.10–0.91; $P = 0.033$, respectively). Expression of sulfotransferase SULT2A1 was associated with prognosis to a similar extent and was validated to be a prognostic factor in two published data sets. We discovered the presence of estradiol-17β 3,17-disulfate (E2S2) in a subset of tumors with particularly poor overall survival. Electron microscopy revealed novel membrane-delimited organelles in only these tumors. By applying cluster analyses of metabolomic data, 3 sulfation-related phenotypes exhibited specific metabolic features unrelated to steroid metabolism.

CONCLUSIONS: MALDI-MSI provides novel insights into the pathophysiology of ACC. Steroid hormone sulfation may be used for prognostication and treatment stratification. Sulfation-related metabolic reprogramming may be of relevance also in conditions beyond the rare ACC and can be directly investigated by the use of MALDI-MSI.

Adrenocortical carcinoma (ACC)[12] is an orphan disease with an annual incidence of between 0.5 and 2 per million inhabitants/year *(1)*, which is in sharp contrast to the high prevalence of adrenocortical adenoma *(2)*. The establishment of international, multicenter consortia has led to a more detailed understanding of the pathogenesis of ACC *(3, 4)* and the identification of clinical prognostic factors including an improved tumor classification *(5, 6)*. It has also enabled collaborative clinical trials *(7, 8)*, and most recently has led to the development of the international European Society of Endocrinology (ESE)/European Network for the Study of Adrenal Tumor (ENSAT) guideline for the diagnosis and treatment

[1] Research Unit Analytical Pathology, German Research Center for Environmental Health, Helmholtz Zentrum München, Neuherberg, Germany; [2] Department of Internal Medicine, Division of Endocrinology and Diabetology, University Hospital Würzburg, Würzburg, Germany; [3] Institute of Pathology, University of Würzburg, Würzburg, Germany; [4] Central Laboratory, University Hospital Würzburg, Würzburg, Germany; [5] Institute of Metabolism and Systems Research, University of Birmingham, Birmingham, UK; [6] Department of General, Visceral, Vascular, and Paediatric Surgery, University Hospital Würzburg, Würzburg, Germany; [7] Comprehensive Cancer Center Mainfranken, University of Würzburg, Würzburg, Germany; [8] MIVENDO Klinik, Hamburg, Germany; [9] University of Sao Paolo, São Paulo, Brazil; [10] Translational Genomics Research Institute (TGen), Phoenix, AZ; [11] Royal North Shore Hospital and The University of Sydney, Sydney, Australia.

* Address correspondence to this author at: Department of Internal Medicine, Division of Endocrinology and Diabetology, University Hospital Würzburg, Oberdürrbacher Str. 6, 97080 Würzburg, Germany. Fax +49-931-201-6039740; e-mail Kroiss_M@ukw.de.

† N. Sun and T. Kunzke contributed equally to this work.

Received April 15, 2019; accepted July 23, 2019.
Previously published online at DOI: 10.1373/clinchem.2019.306043

[12] Nonstandard abbreviations: ACC, adrenocortical carcinoma; ESE, European Society of Endocrinology; ENSAT, European Network for the Study of Adrenal Tumors; MALDI-MSI; MALDI mass spectrometry imaging; FFPE, formalin-fixed, paraffin-embedded; TMA, tissue microarray; ROI, region of interest; MS/MS, tandem mass spectrometry; HMDB, Human Metabolome Database; KEGG, Kyoto Encyclopedia of Genes and Genomes; IHC, immunohistochemistry; STS, steroid sulfatase; SULT, sulfotransferase; TCGA, The Cancer Genome Atlas; E2S, estradiol-17β 3-sulfate; E1S, estrone 3-sulfate; E2S2, estradiol-17β 3,17-disulfate; HR, hazard ratio.

of ACC *(9)*. Genome-wide studies have been performed in ACC to better understand the mechanisms of tumorigenesis, malignancy, and tumor progression *(3, 4, 10)*. However, in approximately 40% of tumors, recurrent genetic driver events have not been identified and novel molecular treatment targets are still scarce.

Tumor-related excess of steroid hormones such as cortisol and sex steroids is the leading clinical finding in 50%–60% of cases of ACC *(11, 12)*, with tumor-induced Cushing syndrome entailing a particularly poor prognosis *(13, 14)*. Importantly, even in ACCs without clinically relevant hormone excess, steroid hormone profiling can be used for diagnosis of malignancy *(15, 16)*.

Although clinical management of ACC in dedicated centers has greatly improved, the assessment of tumor aggressiveness remains one of the major challenges. Even within a given tumor stage, the course of the disease is highly heterogeneous. Because treatment is burdened with significant adverse drug effects, more personalized therapies are required. Genome-wide molecular studies *(3, 4)* have provided only a little novel insight into the mechanisms underlying the variable prognosis and few novel leads for the development of further diagnostic and therapeutic avenues *(17)*.

Molecular phenotyping of tumors at the level of small molecules is an innovative approach that may overcome some of the limitations of genomic and RNA expression data. MALDI mass spectrometry imaging (MALDI-MSI) is a rapidly developing technology that enables the acquisition of molecular images based on the spatially resolved, label-free semiquantitative detection of hundreds to thousands of different molecules such as metabolites in biological samples without prior knowledge of their presence *(18–20)*. Recently it has been demonstrated that meaningful information can also be retrieved from formalin-fixed, paraffin-embedded (FFPE) tissue *(21, 22)*, which greatly facilitates the application of MALDI-MSI in a clinical setting. MALDI-MSI, to the best of our knowledge, has not yet been applied to the study of ACC. We have demonstrated that it is possible to detect steroid hormones as their sulfated metabolites in the tissue of healthy adrenal glands *(23)*, which enabled novel insights into the processes related to steroidogenesis. In this study we focused on steroid hormone sulfation in ACC and investigated associated metabolic events by using tumor prognosis as a marker of tumor biology.

Materials and Methods

TISSUE MICROARRAY PREPARATION

This study was performed as part of the ENSAT registry (https://registry.ensat.org), which was approved by the Ethics Committee of the University of Würzburg (approval numbers 86/03 and 88/11). All patients provided written informed consent. Tissue microarrays (TMAs) were constructed using FFPE tissue samples from 72 ACC patients. Cores from representative tumor areas were identified by an experienced pathologist and 3 cores with 1-mm diameter from each sample were transferred into the microarray.

MALDI-MSI EXPERIMENTS

The TMA samples were cut into 3-μm-thick sections on a microtome (HM 355S, Microm, ThermoScientific) and mounted onto indium tin oxide–coated glass slides. The FFPE sections were incubated at 60 °C for 1 h, deparaffinized in xylene (2 × 8 min), and dried on a hot plate at 37 °C. The matrix solution consisted of 10 g/L 9-AA (9-aminoacridine hydrochloride monohydrate; Sigma-Aldrich) in water/methanol 30:70 (v/v). SunCollect^{TM} automatic sprayer (Sunchrom) was used for matrix application. The flow rates were 10, 20, 30, and 40 μL/min for the first 4 layers. The other 4 layers were applied at 40 μL/min. The MALDI-MSI measurement was performed on a solariX 7T FT-ICR-MS (Bruker Daltonics) in negative ion mode using 50 laser shots per spot at a frequency of 500 Hz. The MALDI-MSI data were acquired over a mass range of *m/z* 50–1000 with 60-μm lateral resolution. Following the MALDI imaging experiments, the matrix was removed with 70% ethanol, and tissue sections were stained with H&E (hematoxylin and eosin). The slides were scanned with a Mirax Desk scanner (Zeiss) with a 20× magnification objective. After the MALDI-MSI measurement, the acquired data underwent spectra processing in FlexImaging v. 4.0 (Bruker). MALDI-MSI data were normalized to the root mean square of all data points. Tumor regions of the ACC samples as regions of interest (ROIs) were annotated. The average spectral data of ROIs were then exported to peak list as .csv files from FlexImaging software.

ON-TISSUE MALDI-MS/MS FOR METABOLITE IDENTIFICATION

For identification of metabolites, on-tissue MS/MS analysis was conducted using CASI (continuous accumulation of selected ions) mode and CID (collision-induced dissociation) in the collision cell by MALDI-FT-ICR-MS. After MS/MS, metabolites were either identified by comparing the observed MS/MS spectra with standard compounds or by matching accurate mass with databases as previously described (ion mode: negative, adduct type: [M-H], [M-H-H2O], mass accuracy ≤8 ppm, METLIN, http://metlin.scripps.edu/; Human Metabolome Database (HMDB), http://www.hmdb.ca/) *(21, 22, 24)*. Pathway analysis was performed with the Kyoto Encyclopedia of Genes and Genomes (KEGG) database (http://www.genome.jp/kegg/).

BIOINFORMATICS AND STATISTICAL ANALYSIS

MATLAB® R2014b (v.7.10.0, Mathworks) was used for preprocessing of MALDI spectra as previously described *(21, 22, 24)*. Mass spectra underwent resampling, smoothing, and baseline subtraction to decrease the data dimensionality and to remove noise-level peaks and artifacts. Peak picking was performed using an adapted version of the LIMPIC (linear MALDI-TOF-MS peak indication and classification) algorithm *(25)* with *m/z* 0.0005 minimum peak width. The signal-to-noise and intensity threshold was set to 2% and 0.01%, respectively. Isotopes were automatically identified and excluded. To identify statistically significant differences in *m/z* values, the peaks were analyzed with the Mann–Whitney *U*-test and corrected for multiple comparisons using the Benjamini–Hochberg correction ($\alpha = 0.05$).

Heatmap-based clustering analysis was performed with MetaboAnalyst 3.0 (http://www.metaboanalyst.ca). Box plots and bar charts were created with GraphPad PRISM v. 5.00 (GraphPad Software). Groups were compared using the Kruskal–Wallis test ($\alpha = 0.05$) and the Dunn multiple comparisons test.

Overall survival was defined as the time from primary surgery to death or last follow-up and was calculated using the Kaplan–Meier method and included 95% CI estimates. Survival curves were compared with the log-rank χ^2 value. In each case, the cutoff point was optimized with respect to the endpoint. Multivariate survival analyses including age, ENSAT tumor stage, and sex were performed by Cox regression modeling, with *P* values calculated by the Wald test. All statistical analyses were performed within the R statistical environment including "Survival" package (R Foundation for Statistical Computing) and *P* values <0.05 were considered statistically significant.

IMMUNOHISTOCHEMISTRY AND IMAGE ANALYSIS

Immunohistochemical (IHC) staining of steroid sulfatase (STS) and sulfotransferases (SULTs) SULT1E1, SULT2A1, and SULT2B1 was performed under standardized conditions on a Discovery XT automated stainer (Ventana Discovery XT Systems, Ventana Medical Systems, Inc.). The respective primary antibodies were anti-STS (HPA002904, dilution 1:50; Sigma-Aldrich), anti-SULT1E1 (HPA028728, dilution 1:25; Sigma-Aldrich), anti-SULT2A1 (HPA041487, dilution 1:50; Sigma-Aldrich), and anti-SULT2B1 (HPA041724, dilution 1:20, Sigma-Aldrich). Following IHC, stained TMA slides were scanned at 20× objective magnification using a digital Mirax Desk slide scanner before import into the image analysis software Definiens Developer XD2 (Definiens AG), as previously described *(26)*. Tumor areas were annotated manually and a rule set was defined and applied to detect and quantify staining intensities in the annotated tumor area.

TRANSMISSION ELECTRON MICROSCOPY

FFPE tissues were deparaffinized, rehydrated, and stained in 2% aqueous osmium tetroxide *(27)*, dehydrated in gradual ethanol (30%–100%) and propylene oxide, embedded in Epon (Merck), and dried for 48 h at 60 °C. Semithin sections were cut and stained with toluidine blue. Ultrathin sections of 50 nm were collected onto 200 mesh copper grids and stained with uranyl acetate and lead citrate before examination by transmission electron microscopy (Zeiss Libra 120 Plus, Zeiss). Pictures were acquired using a Slow Scan CCD-camera and iTEM software (Olympus).

ISOLATION OF DNA FROM FFPE TISSUE AND STS SEQUENCING

A total of 20 μm of full FFPE slides from the corresponding primary tumor block were used to extract DNA with the QIAamp® DNA FFPE Tissue Kit (Qiagen), according to the manufacturer's instructions. Elution occurred in 30-μL H_2O, and DNA quality and concentration were determined with the NanoDrop™ spectrophotometer (Thermo Scientific). Amplification of the mutational hotspot region encompassing the c.1337G>A (p.C446Y) mutation in exon 9 of the STS gene was performed with 20 ng of DNA, and the primers GTCTTGATGCCTGGCTGTTT (forward) and TATTCCCATGGCATAGGTTGC (reverse) were used. The program consisted of 30 cycles with denaturing at 94 °C (30 s), annealing at 58 °C (30 s), and elongation at 72 °C (30 s).

For Sanger sequencing, the same primers were used in the sequencing reaction, and the sequencing results were analyzed with the GenomeLab Genetic Analysis System (Beckman-Coulter, ABSciex).

IN SILICO ANALYSES

Data from The Cancer Genome Atlas (TCGA) analysis of 91 ACCs *(4)* were retrieved from the Broad Institute Genome Data Analysis Center FireBrowse portal (http://firebrowse.org/?cohort=ACC). RNA sequencing data were log normalized, and expression profiling for selected genes was performed using Prism 6 for Mac Software (GraphPad). Somatic mutation data of the same samples were screened using the Integrated Genomic Viewer 2.3.67 for Mac based on the human genome assembly GRCh37 (hg19). Gene expression microarray data from 33 ACCs *(10)* were downloaded from the Gene Expression Omnibus Repository (https://www.ncbi.nlm.nih.gov/geo/query/acc.cgi?acc=GSE10927), and expression differences between the 2 groups were analyzed using Prism 6 for Mac Software.

Survival analyses were performed with GraphPad Prism 6 for Mac using the clinical annotations provided within the individual files.

Table 1. Clinicopathological parameters of the patient cohort.

Characteristic	Number (%) of patients or median (range)
Number of patients	72
Female sex, number (%)	42 (58)
Age at initial diagnosis, years	52 (12–77)
ENSAT tumor stage at initial diagnosis, number (%)	
I	8 (11)
II	32 (45)
III	16 (22)
IV	16 (22)
Main endocrine activity at initial diagnosis, number (%)	
Glucocorticoid excess	24 (34)
Androgen/estrogen excess	3 (4)
Mineralocorticoid excess	3 (4)
None	11 (15)
Not available	31 (43)
Histopathology	
Ki67, n = 49	
<10%	22 (45)
10%–19%	13 (26.5)
≥20%	14 (28.5)
Weiss score, n = 55	5 (2–8)
Tumor sample type	
primary tumor	59 (82)
local recurrence	4 (6)
distant recurrence	9 (12)

Results

SAMPLE DESCRIPTION AND DATA ACQUISITION

Overall, 72 samples of histologically confirmed ACC with full clinical annotation were studied. Detailed clinical characteristics are given in Table 1. The workflow of integrated phenotyping of ACC including IHC, MALDI-MSI, and transmission electron microscopy is summarized in Fig. 1 in the Data Supplement that accompanies the online version of this article at http://www.clinchem.org/content/vol65/issue10.

Within the mass range of *m/z* 50–1000, approximately 2000 individual MS peaks per pixel could be resolved within each tissue examined. In total, 1141 metabolites were annotated through the HMDB (http://www.hmdb.ca/), which covered 94 KEGG metabolic pathways (http://www.genome.jp/kegg/).

IDENTIFICATION OF SULFATED CHOLESTEROL AND STEROID HORMONES

We identified cholesterol sulfate, pregnenolone sulfate, estradiol-17β 3-sulfate (E2S), and estrone 3-sulfate (E1S) by comparing *m/z* values with public databases with a mass error below 4 ppm and validated metabolites with MS/MS (Fig. 2 in the online Data Supplement). A strong correlation between the abundance of E2S and E1S was observed in all samples (Pearson r 0.9618; $P < 0.001$).

In order to expand the spectrum of sulfated steroids beyond known steroid sulfates, we interrogated mass spectra for the calculated *m/z* of disulfated adducts by use of a mass increment of 159.9136 Da to the molecular weight of native steroid hormones. As a result, we discovered the [M-H-H_2O] adduct of estradiol-17β 3,17-disulfate (E2S2) in 6 samples, which was validated by MS/MS (Fig. 2 in the online Data Supplement). No correlation was found between the abundance of any of the sulfated hormones in tissue and clinical or laboratory data of tumoral hormone excess (n = 41 with hormone data; χ^2-test, $P = 0.909$).

IMPACT OF SULFATED ESTROGEN SPECIES ON PROGNOSIS

To determine whether the abundance of E2S and E1S and the presence or absence of E2S2 was associated with tumor aggressiveness, we performed Kaplan–Meier analyses with overall survival as endpoint. Because our setup of MALDI-MSI experiments provided relative abundance of marker molecules, we optimized the cutoff for intensities with respect to the overall survival endpoint (≤0.36 for E1S and ≤0.31 for E2S). We found high abundance of E1S (Fig. 1A) to be significantly associated with more favorable prognosis [hazard ratio (HR) 0.22; 95% CI, 0.07–0.63; log-rank $P = 0.003$] similar to E2S (HR 0.26; 95% CI, 0.10–0.69; log-rank $P = 0.005$; Fig. 1B). Strikingly, the presence of E2S2 (Fig. 1C) was associated with a particularly poor prognosis in comparison to samples in which E2S2 was undetectable (HR 4.35; 95% CI, 1.61–11.74; log-rank $P = 0.001$).

To correct for known or potential factors associated with prognosis, we performed Cox regression modeling with multivariable adjustment for ENSAT-stage, age, and sex that revealed the independent association of marker molecule abundance and presence, respectively, with overall survival (Table 2; E1S: HR 0.30; 95% CI, 0.10–0.91; $P = 0.033$; E2S: HR 0.29; 95% CI, 0.11–0.79; $P = 0.015$; E2S2: HR 4.53; 95% CI, 1.56–13.22; $P = 0.0056$).

SULFOTRANSFERASES AND SULFATASES IN THE MALDI-MSI COHORT

Steroid sulfation is controlled by 2 distinct types of enzymes: (*a*) SULTs that catalyze the sulfation and (*b*) STS that catalyzes desulfation of steroid hormones. To determine the expression of these enzymes we performed IHC staining

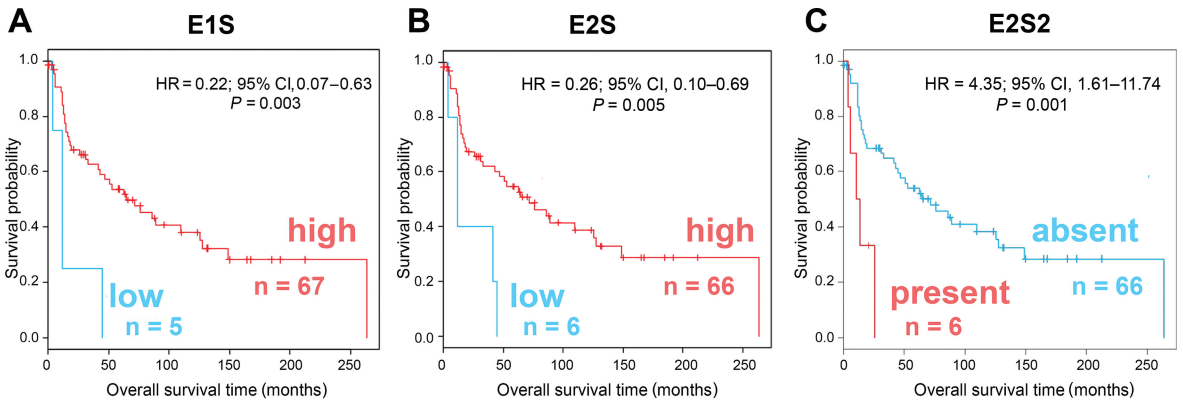

Fig. 1. Kaplan–Meier plots of overall survival.

Overall survival in dependence of high (red) vs low (blue) abundance of (A) E1S and (B) E2S. (C), Overall survival depending on the absence (blue) or presence (red) of E2S2.

and quantification of SULTs (SULT2A1, SULT2B1, and SULT1E1) and sulfatase (STS) expression.

For each enzyme, we found variable expression between tumor samples (for examples, see Fig. 2 A–D) and significant associations with overall survival for SULT2A1 (HR 0.26; 95% CI, 0.10–0.70; log-rank P = 0.004), SULT1E1 (HR 0.41; 95% CI, 0.17–0.99; log-rank P = 0.043), and STS (HR 0.31; 95% CI, 0.09–1.03; log-rank P = 0.043) with a strong trend for SULT2B1 (HR 0.49; 95% CI, 0.24–1.02; logrank P = 0.050; Fig. 2 A–D). Spearman correlation showed strong positive correlations between STS, SULT1E1, and SULT2B1. SULT2A1 was not correlated with any of the other enzymes examined (see Fig. 3 in the online Data Supplement).

To determine whether the occurrence of E2S2 is explained by inactivating mutations in STS, we performed Sanger sequencing of the STS coding sequence in 5/6 samples with presence of E2S2 and sufficient DNA available. We found wild type in all samples.

SULFATION-RELATED ENZYME EXPRESSION AND STEROID SULFATION IN PUBLISHED DATA SETS

To challenge our findings, we analyzed the expression of all SULTs and STS at the mRNA level by using in silico

Table 2. Cox proportional hazard modeling.

	Univariate		Multivariate	
	P value[a]	HR (95% CI)	*P value*	HR (95% CI)
E1S	0.0049	0.22 (0.07-0.63)	0.033	0.30 (0.10-0.91)
ENSAT stage	<0.0001	1.96 (1.41-2.72)	0.0002	2.05 (1.41-2.98)
Age	0.97	1.00 (0.98-1.02)	0.81	1.00 (0.98-1.02)
Sex	0.93	1.02 (0.58-1.80)	0.92	0.97 (0.52-1.80)
E2S	0.0068	0.26 (0.10-0.69)	0.015	0.29 (0.11-0.79)
ENSAT stage	<0.0001	1.96 (1.41-2.72)	<0.0001	2.10 (1.45-3.04)
Age	0.97	1.00 (0.98-1.02)	0.82	1.00 (0.98-1.02)
Sex	0.93	1.02 (0.58-1.80)	0.99	1.00 (0.53-1.87)
E2S2	0.0037	4.35 (1.61-11.74)	0.0056	4.53 (1.56-13.22)
ENSAT stage	<0.0001	1.96 (1.41-2.72)	0.0001	2.05 (1.43-2.94)
Age	0.97	1.00 (0.98-1.02)	0.52	1.01 (0.99-1.03)
Sex	0.93	1.02 (0.58-1.80)	0.90	0.96 (0.51-1.80)

[a] *P* values <0.05 were considered statistically significant.

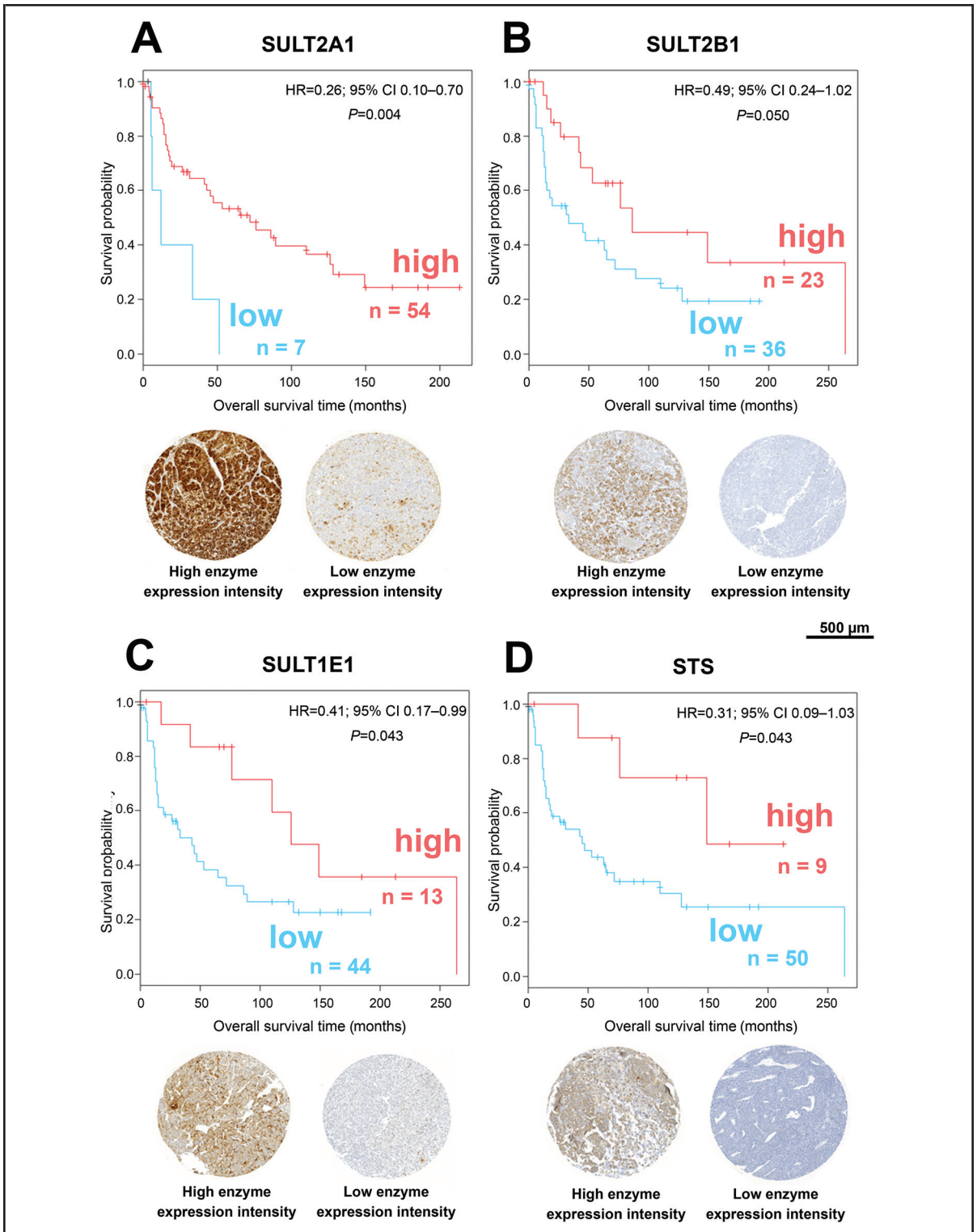

Fig. 2. Enzymes related to steroid hormone sulfation and their impact on survival.

(A–D) Kaplan–Meier plots of high (red) vs low (blue) expression of indicated enzymes. Representative examples of TMA core sections with high and low staining intensities for (A) SULT2A1, (B) SULT2B1, (C) SULT1E1, (D) STS.

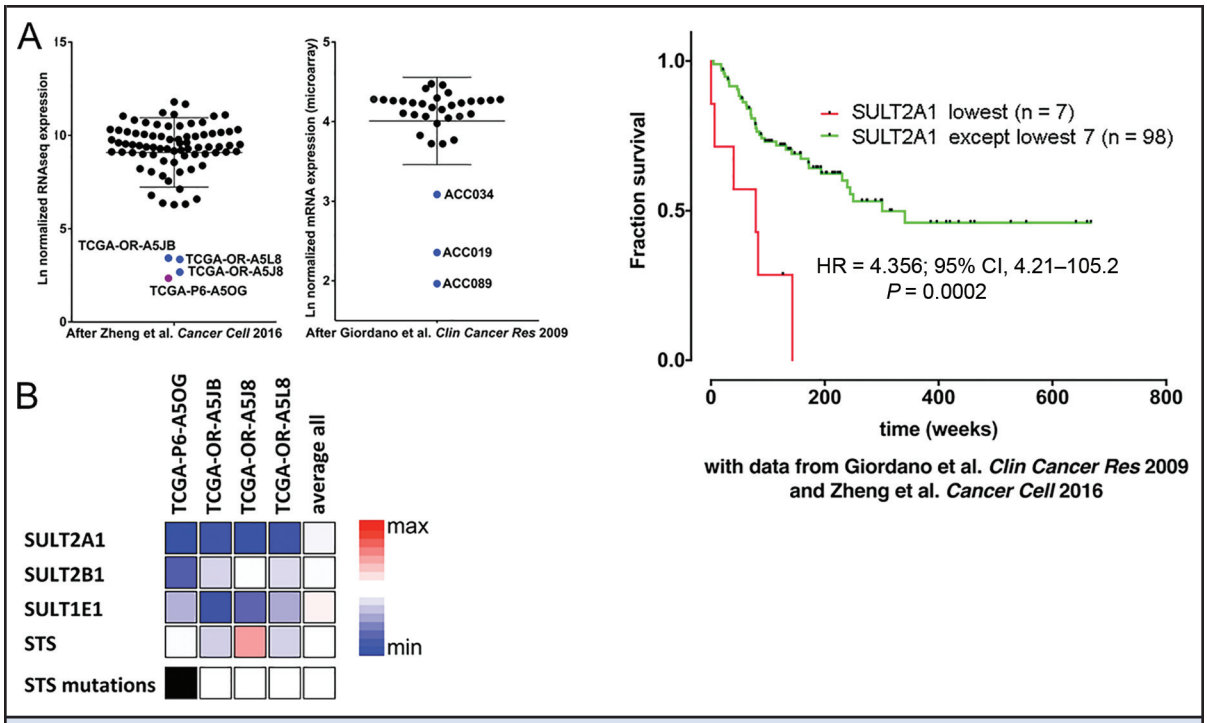

Fig. 3. External validation of sulfation enzyme expression in the TCGA *(4)* and University of Michigan *(10)* data sets.

(A), Normalized mRNA expression determined by RNA-sequencing in the TCGA (left panel) and by gene expression microarray in the University of Michigan series (right panel). Outliers of SULT2A1 are colored. Indicated samples from the TCGA cohort were analyzed for the presence of E2S2 by MALDI MSI. (B), Expression of indicated enzymes at mRNA-level in the 4 TCGA cases studied. Blue indicates decreased and red increased expression of enzymes in comparison to the mean expression of the respective enzyme in the entire data set. Presence of the inactivating STS mutation p.C446Y is indicated in black. (C), Kaplan–Meier Plot of overall survival of the outlier cases with low SULT2A1 expression vs all other samples in a pooled analysis of the TCGA and the University of Michigan cohort.

data of the ACC cohort in TCGA *(4)* and the study by Giordano et al. *(10)*. In both independent cohorts, SULT2A1 expression in ACC was characterized by an outlier group of 4 out of 79 and 3 out of 24 cases, respectively, with extremely low enzyme expression (Fig. 3A). We obtained tissue samples from the 4 TCGA cases, analyzed full tissue sections for marker metabolites, and found 1 sample (TCGA-P6-A5OG) to have detectable E2S2. STS was mutated (c1337G>A, pC446Y, rs137853166) in this sample only and, in addition, the sample also exhibited low expression of SULT2B1 and SULT1E1 mRNA (Fig. 3B). Kaplan–Meier analysis of survival demonstrated significantly less favorable survival for the 7 patients with low SULT2A1 expression in the combined TCGA and Giordano cohorts (78.7 ± 55.7 vs 300.7 ± 149.3 weeks; log-rank $P = 0.0002$; Fig. 3C).

METABOLIC REPERCUSSIONS ASSOCIATED WITH ESTRADIOL SULFATION

Tissue samples were stratified into low-intensity E2S (n = 5; phenotype 1; peak intensity of E2S ≤0.31), high intensity E2S (n = 61; phenotype 2; peak intensity of E2S >0.31), and presence of E2S2 (n = 6; phenotype 3; peak intensity of E2S2 >0). Hierarchical cluster analysis revealed a clear separation of 3 phenotypes (Fig. 4A). Discriminative *m/z* peaks were annotated and pathway mapping was performed. We found amino sugar metabolism (Fig. 4B) and purine metabolism (Fig. 4C) to be distinctive between the 3 phenotypes.

TRANSMISSION ELECTRON MICROSCOPY

To determine whether the different steroid-sulfation phenotypes are associated with changes at the ultrastructural level, we performed transmission electron microscopy analyses of 6 samples with the presence of E2S2 and 3 patients with a high abundance of E2S for comparison. We found the presence of multiple membrane-delimited vacuoles containing an amorphous material in all patient samples with presence of E2S2 (Fig. 4D). Those vacuoles were absent in patients with a high abundance of E2S.

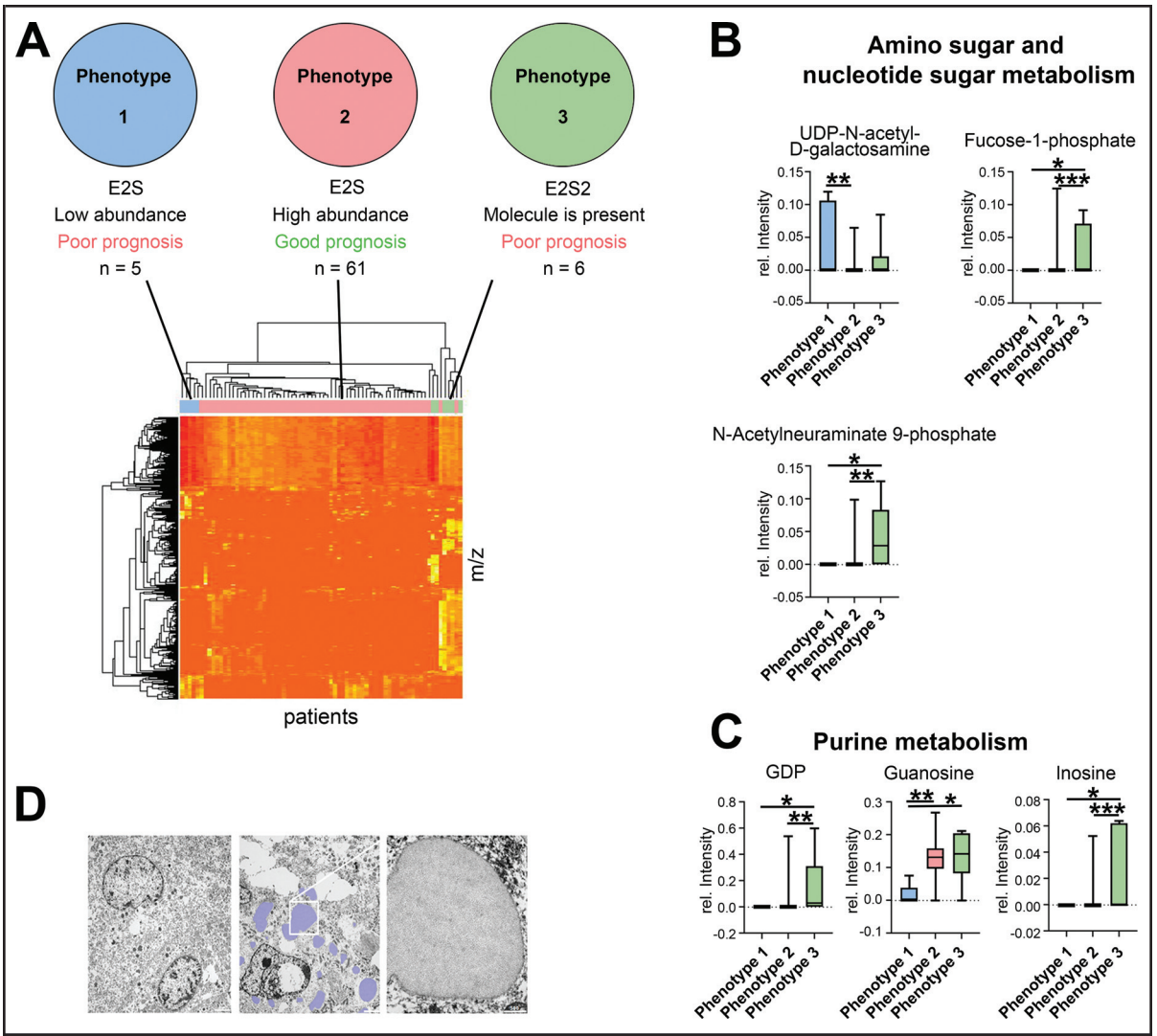

Fig. 4. Ultrastructural and metabolic pathways associated with steroid hormone sulfation phenotypes.

(A), Hierarchical cluster analysis of m/z species show a clear separation of phenotype 1, phenotype 2, and phenotype 3. (B), UDP-N-acetyl-D-galactosamine, fucose-1-phosphate, and N-acetylneuraminate 9-phosphate from amino sugar and nucleotide sugar metabolism. (C), guanosine diphosphate (GDP), guanosine, and inosine from purine metabolism. (D), electron microscopy of tissue samples of phenotype 1 (left panel) and phenotype 3 (center panel) with vacuoles in phenotype 3 samples highlighted in blue (right panel: enlarged ROI). Kruskal–Wallis test ($\alpha = 0.05$) and Dunn multiple comparisons test were used for statistical analysis (*$P < 0.05$, **$P < 0.01$, ***$P < 0.001$, ****$P < 0.0001$).

Discussion

Previously we have described the detection of distinct steroid hormone metabolites in the tissue of healthy adrenal glands by MALDI-MSI *(23)*. In this study, we found certain steroid hormone sulfates to be strongly associated with prognosis in ACC. Accordingly, protein expression levels of sulfation-related enzymes also were found to be positively associated with more favorable prognosis. To the best of our knowledge, this is the first description of hormone detection in tissue that may also serve as a biomarker. In body fluids, steroid hormones are already clinically useful for the diagnosis of endocrine disease, and by combining several steroid hormone metabolites, rare malignant ACCs can be reliably identified *(15, 16)*. Steroid excess in ACC is generally associated with unfavorable survival *(14)*, but steroid hormones in ACC tissue have not been studied before.

By using MALDI-MSI, we detected only a relatively small number of steroid metabolites in the FFPE tissue,

which is obviously owing to the fixation and embedding procedure. Nevertheless the abundance of both E1S and E2S was informative and appears to reflect tumor biology because of its association with prognosis. Indeed, from our point of view, it is reasonable to choose FFPE samples because of their routine availability and the potential of upscaling by utilization of TMAs. In the future, this strategy may enable high-throughput MALDI-MSI approaches and pave the way for routine application in modern pathology.

The association of a more favorable overall survival with a high abundance of both sulfates and their mutual correlation supports the idea that active steroid sulfation is a marker of a biologically less aggressive phenotype of ACC. Accordingly, SULT protein expression was similarly associated with better prognosis. Steroid hormone sulfates have long been regarded as inactive metabolites because they cannot activate classical steroid receptors and they exhibit low membrane permeation owing to their hydrophilic properties. It has been recognized more recently that sulfation of steroid hormones enables additional levels of regulation beyond the feedback circuits of the hypothalamus–pituitary–gonadal and hypothalamus–pituitary–adrenal axes. Thus, steroid sulfates constitute a large pool of biologically inactive steroids that can be activated in target tissue by desulfation. Within the target cells, hydrolysis occurs by STS *(28)*. Dysregulation of steroid sulfation and desulfation is associated with steroid-dependent cancers, polycystic ovary syndrome, and X-linked ichthyosis *(29)*. The family of SULTs is characterized by relatively broad substrate specificity. Although SULT1E1 has the highest affinity to estrogens and therefore can counteract estrogen receptor binding in target tissues *(30)*, SULT2A1 catalyzes sulfonation of not only DHEA (dehydroepiandrosterone) but also of estrogens *(29, 31, 32)*. In our study, expression of SULT2A1 was associated with survival in a similar manner as the sulfated products themselves, suggesting that this enzyme—which was expressed at highest levels in ACC samples—is the enzyme responsible for E1S and E2S synthesis.

Numerous steroid hormone sulfates can be expected theoretically through the action of steroid SULTs *(33)*. It is noteworthy that in a particular subset of tumors (phenotype 3), sulfation of estradiol at the 17-OH group occurs in addition to the physiological 3-position. In vitro studies have previously demonstrated that preferential sulfation of estradiol at the 17-OH group can result from allosteric modulators of SULT2A1 *(32)*. Available in vitro data have shown that E2S2 is a minor by-product of SULT2A1 activity and, hence, additional factors are likely to contribute to the high abundance of this uncommon metabolite in ACC cells. Whereas it is clear that E2S2 is not a substrate of the SLC10A6 (sodium-dependent organic anion transporter) *(34)*, which catalyzes estrogen sulfate uptake in target tissues, the efflux of steroid sulfates from adrenal cortex cells has not been investigated in detail. However, it appears that disulfates are poor substrates of STS *(35)* and this may contribute to the intracellular accumulation of E2S2. This intracellular accumulation of E2S2 is supported by the electron microscopic detection of membrane-delimited organelles only in E2S2-positive tumors.

It is a strength of this study that the association of SULT2A1 expression with prognosis could be replicated in 2 unrelated published data sets. Remarkably, the proportion of tumors with low SULT2A1 expression is similar across studies. We could not compare the abundance of E1S and E2S in the 4 TCGA samples as we have done in our TMAs. However, we found 1 particular sample with phenotype 3 that also had remarkably low expression of other SULTs, and a somatic mutation in the STS gene was present that was already described as a functional germline mutation associated with X-linked ichthyosis *(36)*.

Whereas a causative role of steroid sulfation cannot be inferred from our data, our tissue metabolomics analysis points toward pathway alteration in several processes unrelated to steroidogenesis. It is noteworthy that both purine metabolism and amino sugar metabolism exhibit significant phenotype-specific differences. This suggests that impaired sulfation may impact both upstream and downstream pathways such as glycosylation. UDP-N-acetyl galactosamine, which we found to be increased in phenotype 1, is the starting moiety of protein O-glycosylation, whereas fucose phosphate and N-acetyl-neuraminate-9-phosphate, which were present at higher levels in phenotype 3 vs both other phenotypes, play a role in specific glycosylated macromolecules. It is beyond the scope of this study to clarify the contribution of glycosylation and purine metabolism. In particular, the groups with phenotype 1 and 3 are relatively small. However, our findings highlight pathways that are not usually accessible with other techniques and demonstrate the power of tissue phenotyping by MALDI-MSI in clinically relevant settings. Yet this technology has to prove its value in routine clinical diagnostics.

In the future era of more personalized ACC treatment *(3, 17)*, the discovery of phenotypes with impaired steroid hormone sulfation at tumoral level and their repercussions throughout the related pathways might pave the way toward novel treatment approaches in this devastating disease. Underlying mechanisms may also be relevant in other malignancies and will be worth further investigations.

Author Contributions: *All authors confirmed they have contributed to the intellectual content of this paper and have met the following 4 requirements: (a) significant contributions to the conception and design,*

acquisition of data, or analysis and interpretation of data; (b) drafting or revising the article for intellectual content; (c) final approval of the published article; and (d) agreement to be accountable for all aspects of the article thus ensuring that questions related to the accuracy or integrity of any part of the article are appropriately investigated and resolved.

Authors' Disclosures or Potential Conflicts of Interest: *Upon manuscript submission, all authors completed the author disclosure form. Disclosures and/or potential conflicts of interest:*

Employment or Leadership: None declared.
Consultant or Advisory Role: None declared.
Stock Ownership: None declared.
Honoraria: None declared.
Research Funding: S. Sbiera, the Else Kröner-Fresenius-Stiftung (2016 A96); M. Fassnacht, the Deutsche Forschungsgemeinschaft (DFG, German Research Foundation) project numbers 314061271–TRR 205 (project S01), FA 466/4-2, the Deutsche Krebshilfe (no. 70112617); A. Walch, the Deutsche Forschungsgemeinschaft (DFG, German Research Foundation) project numbers 314061271–TRR 205 (project S01), the Deutsche Krebshilfe (no. 70112617); M. Kroiss, the Deutsche Forschungsgemeinschaft (DFG, German Research Foundation) project numbers 314061271–TRR 205 (project B16), KR4371/1-2, the Else Kröner-Fresenius-Stiftung (2016 A96), the Deutsche Krebshilfe (no. 70112617).
Expert Testimony: None declared.
Patents: None declared.

Role of Sponsor: The funding organizations played no role in the design of study, choice of enrolled patients, review and interpretation of data, and final approval of manuscript.

Acknowledgments: The authors thank Michaela Haaf, Martina Zink and Kevin Eck for their continuous support in maintaining the ENSAT registry and biobank at the University Hospital Würzburg and all ACC patients for their participation in the ENSAT registry. The authors thank Claudia-Marieke Pflüger, Ulrike Buchholz, Gabriele Mettenleiter, and Andreas Voss from the Research Unit Analytical Pathology for providing technical assistance.

References

1. Kerkhofs TM, Verhoeven RH, Van der Zwan JM, Dieleman J, Kerstens MN, Links TP, et al. Adrenocortical carcinoma: a population-based study on incidence and survival in the Netherlands since 1993. Eur J Cancer 2013;49:2579–86.
2. Fassnacht M, Arlt W, Bancos I, Dralle H, Newell-Price J, Sahdev A, et al. Management of adrenal incidentalomas: European Society of Endocrinology clinical practice guideline in collaboration with the European Network for the Study of Adrenal Tumors. Eur J Endocrinol 2016;175:G1–34.
3. Assie G, Letouze E, Fassnacht M, Jouinot A, Luscap W, Barreau O, et al. Integrated genomic characterization of adrenocortical carcinoma. Nat Genet 2014;46:607–12.
4. Zheng S, Cherniack AD, Dewal N, Moffitt RA, Danilova L, Murray BA, et al. Comprehensive pan-genomic characterization of adrenocortical carcinoma. Cancer Cell 2016;29:723–36.
5. Fassnacht M, Johanssen S, Quinkler M, Bucsky P, Willenberg HS, Beuschlein F, et al. Limited prognostic value of the 2004 International Union Against Cancer staging classification for adrenocortical carcinoma: proposal for a revised TNM classification. Cancer 2009;115:243–50.
6. Libe R, Borget I, Ronchi CL, Zaggia B, Kroiss M, Kerkhofs T, et al. Prognostic factors in stage III-IV adrenocortical carcinomas (ACC): an European Network for the Study of Adrenal Tumor (ENSAT) study. Ann Oncol 2015;26:2119–25.
7. Fassnacht M, Terzolo M, Allolio B, Baudin E, Haak H, Berruti A, et al. Combination chemotherapy in advanced adrenocortical carcinoma. N Engl J Med 2012;366:2189–97.
8. Fassnacht M, Berruti A, Baudin E, Demeure MJ, Gilbert J, Haak H, et al. Linsitinib (OSI-906) versus placebo for patients with locally advanced or metastatic adrenocortical carcinoma: a double-blind, randomised, phase 3 study. Lancet Oncol 2015;16:426–35.
9. Fassnacht M, Dekkers OM, Else T, Baudin E, Berruti A, de Krijger R, et al. European Society of Endocrinology clinical practice guidelines on the management of adrenocortical carcinoma in adults, in collaboration with the European Network for the Study of Adrenal Tumors. Eur J Endocrinol 2018;179:G1–46.
10. Giordano TJ, Kuick R, Else T, Gauger PG, Vinco M, Bauersfeld J, et al. Molecular classification and prognostication of adrenocortical tumors by transcriptome profiling. Clin Cancer Res 2009;15:668–76.
11. Johanssen S, Hahner S, Saeger W, Quinkler M, Beuschlein F, Dralle H, et al. Deficits in the management of patients with adrenocortical carcinoma in Germany. Dtsch Arztebl Int 2010;107:885–91.
12. Else T, Kim AC, Sabolch A, Raymond VM, Kandathil A, Caoili EM, et al. Adrenocortical carcinoma. Endocr Rev 2014;35:282–326.
13. Abiven G, Coste J, Groussin L, Anract P, Tissier F, Legmann P, et al. Clinical and biological features in the prognosis of adrenocortical cancer: poor outcome of cortisol-secreting tumors in a series of 202 consecutive patients. J Clin Endocrinol Metab 2006;91:2650–5.
14. Berruti A, Fassnacht M, Haak H, Else T, Baudin E, Sperone P, et al. Prognostic role of overt hypercortisolism in completely operated patients with adrenocortical cancer. Eur Urol 2014;65:832–8.
15. Arlt W, Biehl M, Taylor AE, Hahner S, Libe R, Hughes BA, et al. Urine steroid metabolomics as a biomarker tool for detecting malignancy in adrenal tumors. J Clin Endocrinol Metab 2011;96:3775–84.
16. Schweitzer S, Kunz M, Kurlbaum M, Vey J, Kendl S, Deutschbein T, et al. Plasma steroid metabolome profiling for the diagnosis of adrenocortical carcinoma. Eur J Endocrinol 2019;180:117–25.
17. Lippert J, Appenzeller S, Liang R, Sbiera S, Kircher S, Altieri B, et al. Targeted molecular analysis in adrenocortical carcinomas: a strategy toward improved personalized prognostication. J Clin Endocrinol Metab 2018;103:4511–23.
18. Norris JL, Caprioli RM. Analysis of tissue specimens by matrix-assisted laser desorption/ionization imaging mass spectrometry in biological and clinical research. Chem Rev 2013;113:2309–42.
19. Walch A, Rauser S, Deininger SO, Hofler H. MALDI imaging mass spectrometry for direct tissue analysis: a new frontier for molecular histology. Histochem Cell Biol 2008;130:421–34.
20. Miura D, Fujimura Y, Wariishi H. In situ metabolomic mass spectrometry imaging: recent advances and difficulties. J Proteomics 2012;75:5052–60.
21. Ly A, Buck A, Balluff B, Sun N, Gorzolka K, Feuchtinger A, et al. High-mass-resolution MALDI mass spectrometry imaging of metabolites from formalin-fixed paraffin-embedded tissue. Nat Protoc 2016;11:1428–43.
22. Buck A, Ly A, Balluff B, Sun N, Gorzolka K, Feuchtinger A, et al. High-resolution MALDI-FT-ICR MS imaging for the analysis of metabolites from formalin-fixed, paraffin-embedded clinical tissue samples. J Pathol 2015;237:123–32.
23. Sun N, Wu Y, Nanba K, Sbiera S, Kircher S, Kunzke T, et al. High-resolution tissue mass spectrometry imaging reveals a refined functional anatomy of the human adult adrenal gland. Endocrinology 2018;159:1511–24.
24. Sun N, Ly A, Meding S, Witting M, Hauck SM, Ueffing M, et al. High-resolution metabolite imaging of light and dark treated retina using MALDI-FTICR mass spectrometry. Proteomics 2014;14:913–23.
25. Mantini D, Petrucci F, Pieragostino D, Del Boccio P, Di Nicola M, Di Ilio C, et al. LIMPIC: a computational method for the separation of protein MALDI-TOF-MS signals from noise. BMC Bioinformatics 2007;8:101.
26. Feuchtinger A, Stiehler T, Jutting U, Marjanovic G, Luber B, Langer R, Walch A. Image analysis of immunohistochemistry is superior to visual scoring as shown for patient outcome of esophageal adenocarcinoma. Histochem Cell Biol 2015;143:1–9.
27. Dalton AJ. A chrome-osmium fixative for electron microscopy. Anat Rec 1955;121:281.
28. Geyer J, Bakhaus K, Bernhardt R, Blaschka C, Dezhkam Y, Fietz D, et al. The role of sulfated steroid hormones in reproductive processes. J Steroid Biochem Mol Biol 2017;172:207–21.
29. Mueller JW, Gilligan LC, Idkowiak J, Arlt W, Foster PA. The regulation of steroid action by sulfation and desulfation. Endocr Rev 2015;36:526–63.
30. Cole GB, Keum G, Liu J, Small GW, Satyamurthy N, Kepe V, Barrio JR. Specific estrogen sulfotransferase (SULT1E1) substrates and molecular imaging probe candidates. Proc Natl Acad Sci U S A 2010;107:6222–7.
31. Falany CN. Enzymology of human cytosolic sulfotransferases. FASEB J 1997;11:206–16.
32. Wang LQ, James MO. Sulfotransferase 2A1 forms estradiol-17-sulfate and celecoxib switches the dominant product from estradiol-3-sulfate to estradiol-17-sulfate. J Steroid Biochem Mol Biol 2005;96:367–74.

33. McLeod MD, Waller CC, Esquivel A, Balcells G, Ventura R, Segura J, Pozo OJ. Constant ion loss method for the untargeted detection of bis-sulfate metabolites. Anal Chem 2017;89:1602–9.

34. Grosser G, Bennien J, Sanchez-Guijo A, Bakhaus K, Doring B, Hartmann M, et al. Transport of steroid 3-sulfates and steroid 17-sulfates by the sodium-dependent organic anion transporter SOAT (SLC10A6). J Steroid Biochem Mol Biol 2018;179:20–5.

35. Cook IT, Duniec-Dmuchowski Z, Kocarek TA, Runge-Morris M, Falany CN. 24-hydroxycholesterol sulfation by human cytosolic sulfotransferases: formation of monosulfates and disulfates, molecular modeling, sulfatase sensitivity, and inhibition of liver x receptor activation. Drug Metab Dispos 2009;37:2069–78.

36. Ghosh D. Mutations in X-linked ichthyosis disrupt the active site structure of estrone/DHEA sulfatase. Biochim Biophys Acta 2004;1739:1–4.